THE JOURNAL OF BIOLOGICAL CHEMISTRY VOL. 281, NO. 20, pp. 14173–14183, May 19, 2006
Printed in the U.S.A.

Nitric-oxide Synthase Output State

*DESIGN AND PROPERTIES OF NITRIC-OXIDE SYNTHASE OXYGENASE/FMN DOMAIN CONSTRUCTS**

Received for publication, September 8, 2005, and in revised form, January 31, 2006 Published, JBC Papers in Press, February 3, 2006, DOI 10.1074/jbc.M509937200

Dipak K. Ghosh[‡1], Michael A. Holliday[‡], Clayton Thomas[‡], J. Brice Weinberg[‡], Susan M. E. Smith[§], and John C. Salerno[§2]

From the [‡]Department of Medicine, Duke University and Veterans Affairs Medical Center, Durham, North Carolina 27705 and [§]Department of Biology, Rensselaer Polytechnic Institute, Troy, New York 14853

Mammalian nitric-oxide synthases are large modular enzymes that evolved from independently expressed ancestors. Calmodulin-controlled isoforms are signal generators; calmodulin activates electron transfer from NADPH through three reductase domains to an oxygenase domain. Structures of the reductase unit and its homologs show FMN and FAD in contact but too isolated from the protein surface to permit exit of reducing equivalents. To study states in which FMN/heme electron transfer is feasible, we designed and produced constructs including only oxygenase and FMN binding domains, eliminating strong internal reductase complex interactions. Constructs for all mammalian isoforms were expressed and purified as dimers. All synthesize NO with peroxide as the electron donor at rates comparable with corresponding oxygenase constructs. All bind cofactors nearly stoichiometrically and have native catalytic sites by spectroscopic criteria. Modest differences in electrochemistry *versus* independently expressed heme and FMN binding domains suggest interdomain interactions. These interactions can be convincingly demonstrated via calmodulin-induced shifts in high spin ferriheme EPR spectra and through mutual broadening of heme and FMNH$^{\bullet}$ radical signals in inducible nitric-oxide synthase constructs. Blue neutral FMN semiquinone can be readily observed; potentials of one electron couple (in inducible nitric-oxide synthase oxygenase FMN, FMN oxidized/semiquione couple = +70 mV, FMN semiquinone/hydroquinone couple = −180 mV, and heme = −180 mV) indicate that FMN is capable of serving as a one electron heme reductant. The construct will serve as the basis for future studies of the output state for NADPH derived reducing equivalents.

Nitric-oxide synthases (NOSs)[3] are a family of enzymes that generate nitric oxide (NO) from arginine, requiring 2 mol of O_2 and 1.5 mol of NADPH/mol of NO produced (1–3). The constitutive isoforms, eNOS and nNOS, are regulated by calcium/calmodulin (Ca^{+2}/CaM) (4, 5) and additional inputs including phosphorylation of specific residues (6); the NO produced by constitutive isoforms functions as a molecular signal. A cytokine inducible isoform (iNOS) is calcium insensitive, and produces much larger fluxes of NO as a cytotoxin in immune response (4).

Eukaryotic NOS isoforms are large modular enzymes. The monomer molecular mass is 120–161 kDa; the dimer is the active form (7), and the dimerization interface includes the tetrahydrobiopterin (H_4B) binding site in the oxygenase domain (8). The common elements are the heme and H_4B containing the oxygenase domain and a complex reductase unit homologous to NADPH P450 reductase that consists of a NADPH binding domain, a FAD binding domain, and an FMN binding domain (9–11). The reductase and oxygenase regions are linked by a polypeptide segment containing a CaM binding site (12). Evidence suggests that the oxygenase domain of one monomer is reduced by the reductase unit of the other (13) through an oxygenase domain surface that exposes the corner of the heme (8).

Ca^{+2}/CaM controls constitutive isoforms through regulation of electron transfer between NADPH and heme (14). CaM has little or no effect on the thermodynamics of redox processes in NOS, suggesting that regulation is accomplished through modulation of electron transfer (15–18). A 40–50-residue autoinhibitory insertion in the FMN binding domain marks the major difference between cNOSs and iNOS (19), but electron transfer modulation appears also to involve a much smaller insertion present in the subdomain region as well as C-terminal tail differences (20, 21).

Although no solved structure of the holoenzyme exists, both partial structures and structures of close homologs provide considerable information (22–24). In structures of P450 reductase and NOS reductase domains (22–24), the flavin isoalloxazine ring edges are within 5 Å of each other in the interior of the protein. The available structural and evolutionary information strongly suggests that this conformation can serve as the input state from electrons from NADPH but not as the output state to acceptors such as the oxygenase domain or cytochrome *c*. For example, FMN cannot be docked to within tunneling distance of heme. These enzymes evolved from ancestral systems in which the FMN domain was a separate protein that functioned as a free shuttle before gene fusion events tethered it to the FAD binding domain (25). Available crystal structures show only the input state of the shuttle. Mechanistic information suggests that the limiting step in catalysis is the formation of the output state; NAPDH reduction is 3 orders of magnitude faster than NO production, and cytochrome *c* reduction is intermediate between the two.

A construct containing just the FMN binding domain and the oxygenase domain would facilitate study of the association of these two domains free of the influence of the FAD and NADPH binding domains. An analogous construct has been expressed and characterized for cyto-

* This work was supported by American Heart Association Grant 0365338U (to D. K. G.) and by a grant from the American Diabetes Association (to S. M. E. S. and J. C. S.). The costs of publication of this article were defrayed in part by the payment of page charges. This article must therefore be hereby marked "*advertisement*" in accordance with 18 U.S.C. Section 1734 solely to indicate this fact.

[1] To whom correspondence may be addressed. Tel.: 919-286-0411 (ext. 15249); Fax: 919-286-6891; E-mail: dgx@acpub.duke.edu.

[2] To whom correspondence may be addressed. Tel.: 518-276-6392; Fax: 518-276-2344; E-mail: salerj@rpi.edu.

[3] The abbreviations used are: NOS, nitric-oxide synthase; eNOS, endothelial NOS (NOSIII); iNOS, inducible NOS (NOSII); nNOS, neuronal NOS (NOSI); cNOS, constitutively expressed NOS (eNOS and nNOS); CaM, calmodulin; oxyFMN, oxygenase domain/FMN binding domain construct, as defined in Fig. 2; H_4B, (6*R*,6*S*)-2-amino-4-hydroxy-6-(L-*erythro*-1,2-dihydroxypropyl)-5,6,7,8-tetrahydropteridine (tetrahydrobiopterin); EPPS, 4-(2-hydroxyethyl)-1-piperazinepropanesulfonic acid; MOPS, 3-(*N*-morpholino)propanesulfonic acid; L-NOHA, *N*ω-hydroxy-L-arginine; epr, electron paramagnetic resonance; Bis-tris, 2-[bis(2-hydroxyethyl)amino]-2-(hydroxymethyl)propane-1,3-diol; sq, semiquinone.

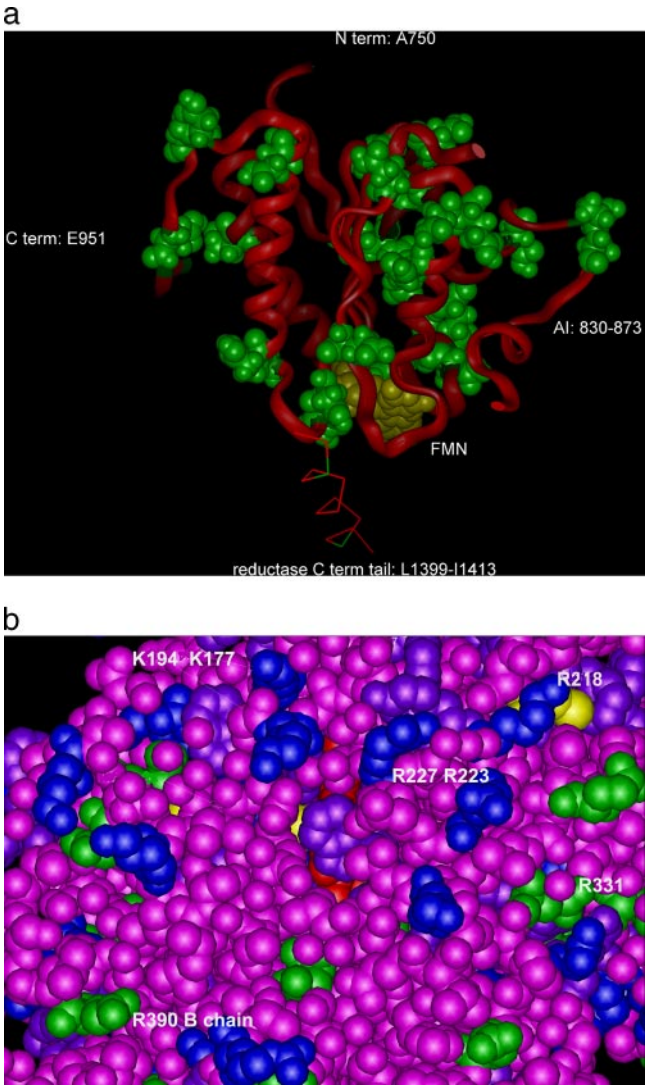

FIGURE 1. *a*, nNOS FMN binding domain showing negatively charged residues in *green solids* on a *red ribbon* marking the main chain. FMN is shown in *solid yellow*. The figure was constructed using information in PDB entries 1AMO and 1TLL (22, 24). *b*, surface of eNOS oxygenase domain showing conserved positive charge array (*dark blue*) surrounding heme (*red*). The figure was constructed using information in PDB entries 3NOS and 1D0O (39, 40).

chrome P450BM-3 from *Bacillus megaterium*, which has a P450 oxygenase domain unrelated to NOS linked to a reductase unit homologous to the corresponding NOS domains (26). P450BM-3 does not bind calmodulin. The *B. megaterium* construct was used to provide a simpler system for kinetic investigations. This communication describes the design and production of an oxyFMN NOS construct and provides preliminary characterization of its properties. We intend to use this construct to characterize the previously described (25) output state of the FMN binding domain of NOS.

MATERIALS AND METHODS

Design of NOS OxyFMN; Strategy and Bacterial Expression Vectors—The oxygenase and FMN binding domains of mammalian NOS have extended surface charge distributions that appear to define interaction surfaces. The surface of the oxygenase domain has a well defined ring of positive charge surrounding the most exposed edge of the heme. The FMN binding site is surrounded by a group of negatively charged residues, but these surfaces cannot interact when the FMN binding domain is associated with the reductase complex. When the constructs described here were originally designed, the reductase structure was not available, but a good approximation was made by modeling based on the structure of P450 reductase (22). Three logical termination points were selected; the shortest construct terminated directly at the end of the final α helix of the FMN binding domain. The constructs described here were designed to include the initial two acidic residues in cNOS of a C-terminal negatively charged element, which closely wrapped the edge of the FMN binding domain (shown on the *left* of Fig. 1*a* terminating as *E951*) before forming the connector to the FAD binding domain. The extended connector was not included in any of the constructs. The *solid green* residues are acidic and define two negatively charged surfaces, including the one facing the viewer.

Fig. 1*b* shows the face of the oxygenase domain in which a corner of the heme, shown in *red*, is exposed. The *dark blue* residues are positively charged, the *green* residues negatively charged, and cysteines are shown in *yellow*.

We decided to truncate the oxygenase domains N-terminally at residue 66 for eNOS, 65 for iNOS, and 290 for nNOS to minimize N-terminal proteolysis during purification, as previously described for oxygenase constructs (27, 28). Fig. 2 shows a schematic sequence alignment for the three constructs used in this study. The C-terminal residues are

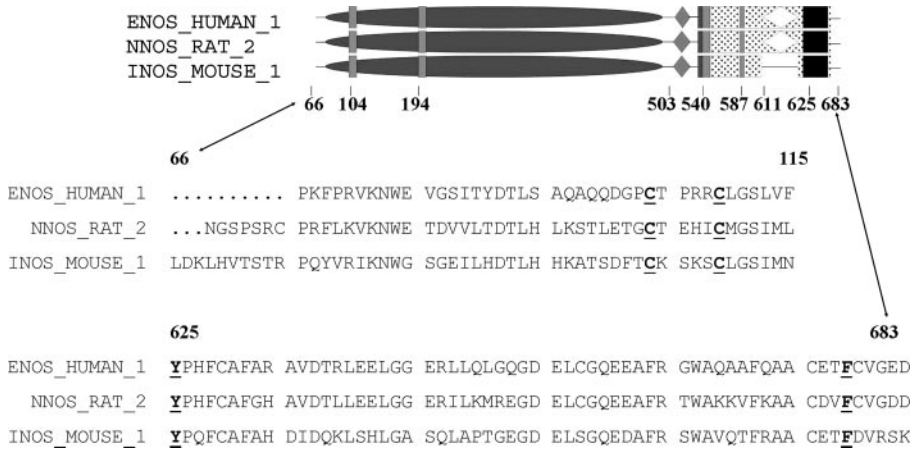

FIGURE 2. **Schematic sequence alignment of oxyFMN constructs showing terminal positions, domains, and some major structural features.** Oxygenase domain at the *left* has binding determinants for Zn^{+2} (mouse iNOS Cys-104 and -109) and heme (mouse iNOS axial Cys-194) indicated; additional sites are included but not marked. These include other residues involved in heme binding and binding sites for pterin and substrate arginine. FMN binding domain at the *right* includes all three regions involved in FMN binding (mouse iNOS residues 540, 587, and 625); cNOS constructs include autoinhibitory insertion within this domain, shown as a *white diamond*. All three constructs include a CaM binding site between the domains (*filled black diamond*). SwissProt accession numbers are P29474 (human eNOS), P29476 (rat nNOS), and P2477 (mouse iNOS).

947 for rat nNOS, 683 for mouse iNOS, and 715 for human eNOS. These constructs include the oxygenase domain with the N-terminal Zn^{+2} binding site for all three cases, and the entire FMN binding domain with five additional associated C-terminal residues beyond the final α helix. This short extension terminates in a pair of conserved acidic residues in cNOSs. All three constructs contain an unmodified and functional CaM binding site. eNOS and nNOS constructs contain the autoinhibitory control element but not the C-terminal tail or the subdomain small insertion hairpin. The schematic shows the location of some major structural features. The aligned sequences of the N- and C-terminal ends of the constructs are shown below to make the exact termination points clear; the entire sequence alignment was not shown to save space.

A Clontech high fidelity PCR kit was employed for cloning of the NOS oxyFMN construct. Using rat nNOS, murine iNOS, and human eNOS cDNA as a template, PCR was used to amplify cDNA encoding residues 291–947 (for rat nNOS), 66–683 (for murine iNOS), and 67–715 (for human eNOS) and to add a sequence coding for a His_6 tag at the N-terminal end of the protein. PCR products were subcloned into the *Escherichia coli* expression vector pCWori+ (27, 29). Δ66 human eNOSox (residues 67–500, the oxygenase domain) was also made by PCR amplification followed by cloning in pCWori+.

Recombinant Protein Production—The pCWori+ vector expressing human eNOS and rat nNOS oxyFMN was transformed into protease-deficient *E. coli* strain BL21DE3 (Novagen) as described for the oxygenase domain (27, 28). Cells were grown in Terrific Broth (Sigma) containing 125 μg/ml ampicillin. Cultures were shaken at 250 rpm at 37 °C until an *A* of 1.0 at 600 nm was reached. Protein expression was induced by adding 0.5 mM isopropyl-β-D-thiogalactopyranoside plus 0.4 mM of the heme precursor δ-aminolevulinic acid, and shaking was continued for 42 h at 22 °C (27). Production of murine iNOS oxyFMN followed a similar procedure, except CaM coexpression was required, and therefore, 40 μg/ml chloramphenicol was added to the culture medium in addition to ampicillin as described for holoiNOS expression (30).

Recombinant Protein Purification—Cells were harvested by centrifugation at 5000 × *g* for 20 min at 4 °C and kept at −80 °C for a day or two. The frozen cell pellet was resuspended in a minimal volume of lysis buffer (40 mM EPPS for murine iNOS, pH 7.6, containing 2 mg/ml lysozyme, 10% glycerol, 150 mM NaCl, 0.5 mM L-Arg 10 μM H_4B, 2 μM FMN, and 1 mM phenylmethylsulfonyl fluoride). For nNOS and eNOS Bis-tris propane was used instead of EPPS for lysis buffer with an otherwise identical composition. Cells were broken by sonication for three 20-s pulses with a 2-min rest on ice between pulses followed by 3 cycles of freezing and thawing as described for NOS holoenzyme (15, 30, 31) Cell debris was removed by centrifugation at 30,000 × *g* for 30 min at 4 °C. The supernatant was applied to a column containing Ni^{+2}-nitrilotriacetic acid-Sepharose 4B metal chelate affinity resin (Novagen) pre-equilibrated with either 40 mM EPPS or Bis-tris propane, pH 7.6, containing 150 mM NaCl, 5% glycerol, and 0.5 mM L-Arg (buffer A). The column was washed with 5 bed volumes of buffer A and then with buffer A plus 25 mM imidazole. Bound protein was eluted by buffer A containing 150–300 mM imidazole. Heme-containing fractions were pooled and concentrated by using centriprep-30 (Millipore).

The concentrated protein was dialyzed at 4 °C against three changes of buffer A containing 4 μM H_4B and either 1 mM dithiothreitol or 2 mM 2-mercaptoethanol. eNOS and nNOS oxyFMN were purified further by using a column containing calmodulin-Sepharose (Amersham Biosciences) equilibrated with 40 mM Bis-tris buffer, pH 7.6, containing 1 mM L-Arg, 3 mM dithiothreitol, 4 μM H_4B, 5% glycerol, and 150 mM NaCl (buffer B), and 2 mM CaCl. The column was washed with buffer B plus 0.5 M NaCl to eliminate nonspecific binding, and nNOS and eNOS were eluted with buffer B containing 4 mM EDTA. The heme-containing fractions were pooled, concentrated, and dialyzed at 4 °C against buffer B containing 0.5 mM L-Arg, 1 mM dithiothreitol, 4 μM H_4B, 2 μM FMN, and 5% glycerol and stored in aliquots at −80 °C until further analysis. Murine iNOS oxyFMN was further purified through a Superdex 200-HR (Amersham Biosciences) gel filtration column. For purification of NOS oxygenase domain, one-step Ni^{+2} affinity purification was done as above except both cell lysis and purification were done in the absence of FMN (27).

NOS Activity—Both oxyFMN and oxygenase domain activity were measured by following H_2O_2-supported oxidation of *N*ω-hydroxy-L-Arg (L-NOHA) at 37 °C for 10 min (32, 33). The reaction was carried out in 100 μl of total volume containing 40 mM EPPS, pH 7.6, 150–500 nM oxyFMN or oxygenase domain protein, 1 mM L-NOHA, 0.5 mM dithiothreitol, 30 mM H_2O_2, 10 units/ml superoxide dismutase, 0.5 mg/ml bovine serum albumin, and variable concentrations of H_4B (0–1000 μM). Reactions were initiated by 30 mM H_2O_2 and stopped by the addition of 1500 units of catalase. Nitrite production was measured by the Griess assay as described previously (27, 32, 33).

Potentiometric Titrations—Titrations were carried out under argon in a side arm vessel essentially as described by Dutton (34), with minor NOS-specific modifications as described by Gao *et al.* (15). Titrations were monitored optically with an Aminco DW2000 scanning dual wavelength spectrometer. Mediators were: methyl viologen, 2 μM; benzyl viologen, 2 μM; safranine O, 1 μM; anthroquinone-2-sulfonate, 2 μM; anthroquinone-2,6-disulfonate, 2 μM; pyocyanine, 1 μM; phenazine methyl sulfate, 2 μM.

Simulations of redox titrations were described in Gao *et al.* (15); here only terms for heme and FMN were retained since the constructs lack an FAD binding domain. Briefly, the Nernst equation describing the redox equilibrium of an electron carrier is

$$Eh = Em + RT/nF \log_{10}(\{\text{oxidized}\}/\{\text{reduced}\}) \quad \text{(Eq. 1)}$$

The redox states for FMN are

$$\text{FMN} \overset{E1}{\longleftrightarrow} \text{FMN(H)}^{\bullet} \overset{E2}{\longleftrightarrow} \text{FMNH}_2 \quad \text{(Eq. 2)}$$

Titrations were simulated using summed contributions from two heme states and three flavin states. At any wavelength these contributions are of the form,

$$A_{\text{heme ox}} = \frac{C_{\text{heme}} \times E_{\text{heme ox}} \times 10^{(\text{Eh-Emheme})F/RT}}{(1 + 10^{(\text{Eh-Emheme})F/RT})} \quad \text{(Eq. 3)}$$

$$A_{\text{heme red}} = \frac{C_{\text{heme}} \times E_{\text{heme red}}}{(1 + 10^{(\text{Eh-Emheme})F/RT})} \quad \text{(Eq. 4)}$$

$$A_{\text{FMN}} = \frac{C_{\text{FMN}} \times E_{\text{FMN}} \times 10^{(\text{Eh-E1FMN})F/RT} \times 10^{(\text{Eh-E2FMN})F/RT}}{(1 + 10^{(\text{Eh-E2FMN})F/RT} + 10^{(\text{Eh-E1FMN})F/RT} \times 10^{(\text{Eh-E2FMN})F/RT})} \quad \text{(Eq. 5)}$$

$$A_{\text{FMNH}^{\bullet}} = \frac{C_{\text{heme}} \times E_{\text{FMNH}^{\bullet}} \times 10^{(\text{Eh-E2FMN})F/RT}}{(1 + 10^{(\text{Eh-E2FMN})F/RT} + 10^{(\text{Eh-E1FMN})F/RT} \times 10^{(\text{Eh-E2FMN})F/RT})} \quad \text{(Eq. 6)}$$

$$A_{FMNH_2} = \frac{C_{heme} \times E_{FMNH_2}}{(1+10^{(Eh-E2FMN)F/RT}+10^{(Eh-E1FMN)F/RT}\times 10^{(Eh-E2FMN)F/RT})} \quad \text{(Eq. 7)}$$

where R is the gas constant, F is the Faraday constant, T is the Kelvin temperature, and RT/F is ~59.6 mV at 25 °C. Variables such as ϵ_{FMN} represent extinction coefficients for hemes and FMN redox states at specific wavelengths; A values are the contributions of individual components to the optical density. Variables of the form C_{heme} represent the total concentration of all heme (or, equivalently, FMN) states, including redox, spin, and conformational states, in rapid equilibrium on the time scale of redox equilibration in the experiment. Eh is the standard potential relative to the hydrogen electrode, and midpoint potentials of one electron couples are specified as Emheme, E1FMN, and E2FMN. E1FMN and E2FMN are the midpoint potentials for the first and second one-electron reductions of FMN. In some cases multiple heme components differing in concentration, extinction coefficient, and midpoint potential have been introduced for simulation purposes.

Stoichiometric titrations were carried out in the same vessel as the potentiometric titrations. The apparatus was not intended to measure the reducing equivalents accurately, but by making small additions of buffered dithionite while monitoring the flavin absorbance at 455 nm, it was possible to observe intermediate reduction states without using a mediator system.

Spectroscopy—Binding of L-Arg, H_4B, and imidazole was monitored by UV-visible spectral perturbation analysis. Light absorbance spectra of the purified NOS oxyFMN proteins were obtained with a Hitachi U2010 spectrometer equipped with computer-assisted data collection software (UV solutions, Wellesley Hills, MA). The NOS-ferrous-CO adduct absorbing at 444 nm was used to quantitate heme protein content by using an extinction coefficient of 74 $mM^{-1}\cdot cm^{-1}$ (35, 36).

Electron paramagnetic resonance spectra were carried out using a Bruker spectrometer with a flowing helium cryostat essentially as previously described (36). Samples were frozen quickly in cold isopentane or liquid nitrogen and kept on liquid nitrogen until the spectra were recorded.

Flavin Content—Flavin content was determined by measuring the absorbance of the released flavin at 450 nm using extinction coefficients of 17 mM^{-1} cm^{-1} for FMN. Twenty μM enzyme in 200 μl of 40 mM Tris-HCl buffer, pH 8.0, was placed in a boiling water bath for 10 min, chilled on ice, and centrifuged at 14,000 rpm for 20 min, and the supernatant was used for FMN quantitation using Sigma FMN as standard. The flavin content for all the NOS isoforms mentioned in the results section is an average of the values measured.

RESULTS

The optical spectra of three oxyFMN constructs are shown in Fig. 3, *A–C*. The heme is primarily in the high spin state after treatment with H_4B and arginine during preparation as indicated by the Soret maximum near 400 nm. Features of the oxidized FMN optical spectrum are visible at 450 and 480 nm. The FMN appears to be more oxidized in these constructs than in freshly isolated holoenzyme, probably because the enzyme lacks an NADPH binding site. A band visible near 650 nm is due to the high spin ferriheme charge transfer band. The broad FMN blue neutral band, extending from 550 to 650 nm, that is characteristic of all three mammalian NOS holoenzymes, is very weak or absent. The spectra of corresponding constructs of the nNOS and iNOS are very similar, but in the eNOS oxyFMN construct a significant minority of the ferriheme remains in the low spin state in the presence of arginine. The *top trace* in Fig. 3*D* shows electron paramagnetic resonance spectra of nNOS oxyFMN construct replete with arginine and H_4B. The high spin features at g = 7.7, 4.1, and 1.76 are very similar to the features of the majority species of the arginine and H_4B replete holoenzyme. There are very low levels of low spin heme (g = 2.4 and 2.2), and almost all the heme is in a single high spin state. In particular, there is almost no g = 6 axial ferriheme signal from heme sites that have lost their thiolate ligand. A small amount of adventitious rhombic ferric (g = 4.3) iron is overlapped with the g = 4.1 feature of the heme. There is no detectable $FMNH^{\bullet}$ radical in the EPR spectra of the construct as isolated, consistent with the optical spectra. A small amount of copper contaminant is visible just above g = 2.

The *second trace* in Fig. 3*D* shows a similar spectrum of iNOS oxyFMN construct. Small differences in the g values of the heme spectra are not detectable in this wide scan (but see Fig. 9). The *lower trace* shows the corresponding spectrum of a nNOS oxyFMN preparation that has been passed through a cycle of reduction with a small amount of dithionite and air oxidized, producing an air stable FMN semiquinone, visible at g = 2, and regenerating the high spin ferriheme. UV-visible spectra of a corresponding experiment are shown in Fig. 6.

All preparations of the eNOS, nNOS, and iNOS oxyFMN constructs contained between 0.9 and 1 heme/mol based on the CO difference spectra (not shown but indistinguishable from the CO difference spectra of holoenzyme and oxygenase domains); all of the heme content measured was in the native thiolate heme complex absorbing near 445 nm, with no detectable 420-nm band. The FMN content measured after extraction from the protein was in all cases at least 90% of the heme content, a difference that could result from loss of FMN during the process. The iNOS construct can be purified in higher yield, probably because it lacks an autoinhibitory element and is less likely to be destroyed by proteolysis. The high level of incorporation of the two major prosthetic groups suggests proper folding during expression.

Because there is no NADPH binding site, none of the oxyFMN constructs exhibit either NO production with NADPH as electron donor or any of the common NADPH reductase activities of NOS holoenzymes. However, oxyFMN constructs of all three isoforms are capable of NO synthesis from *N*-hydroxyarginine (L-NOHA) with peroxide as the electron donor. Fig. 4 shows the ability of all three NOS oxyFMN constructs and their oxygenase domain counterparts to catalyze the H_2O_2-supported nitrite formation from L-NOHA as a function of H_4B concentration (0–1000 μM). The activity of both murine and human eNOS and iNOS oxyFMN is similar to their oxygenase domain activities, whereas nNOS oxyFMN showed increased activity compared with that of its oxygenase counterpart. The dependence of NO formation on H_4B concentration is substantially the same for oxyFMN and oxygenase domain preparations. H_4B is not a reactant, since it is substoichiometric with NO production, but the requirement for full activity is greater than expected from the K_d, which is very low. H_2O_2-supported nitrite formation from L-NOHA by NOS oxyFMN also depends on H_4B concentration at similar H_4B levels, as reported earlier for the oxygenase domain and holoprotein (32, 33). The requirement for H_4B has not been elucidated but appears to be related to the use of peroxide as reductant. The activity measured by this method reflects the full functionality of the oxygenase domain catalytic site after expression.

Purified NOS oxyFMN derived from all three isoforms migrates as a dimer during gel filtration analysis (data not shown) without significant aggregation or monomer formation. The 280-nm/Soret absorbance ratio is ~2.2–2.5 in 80–90% pure preparations and serves as a routine

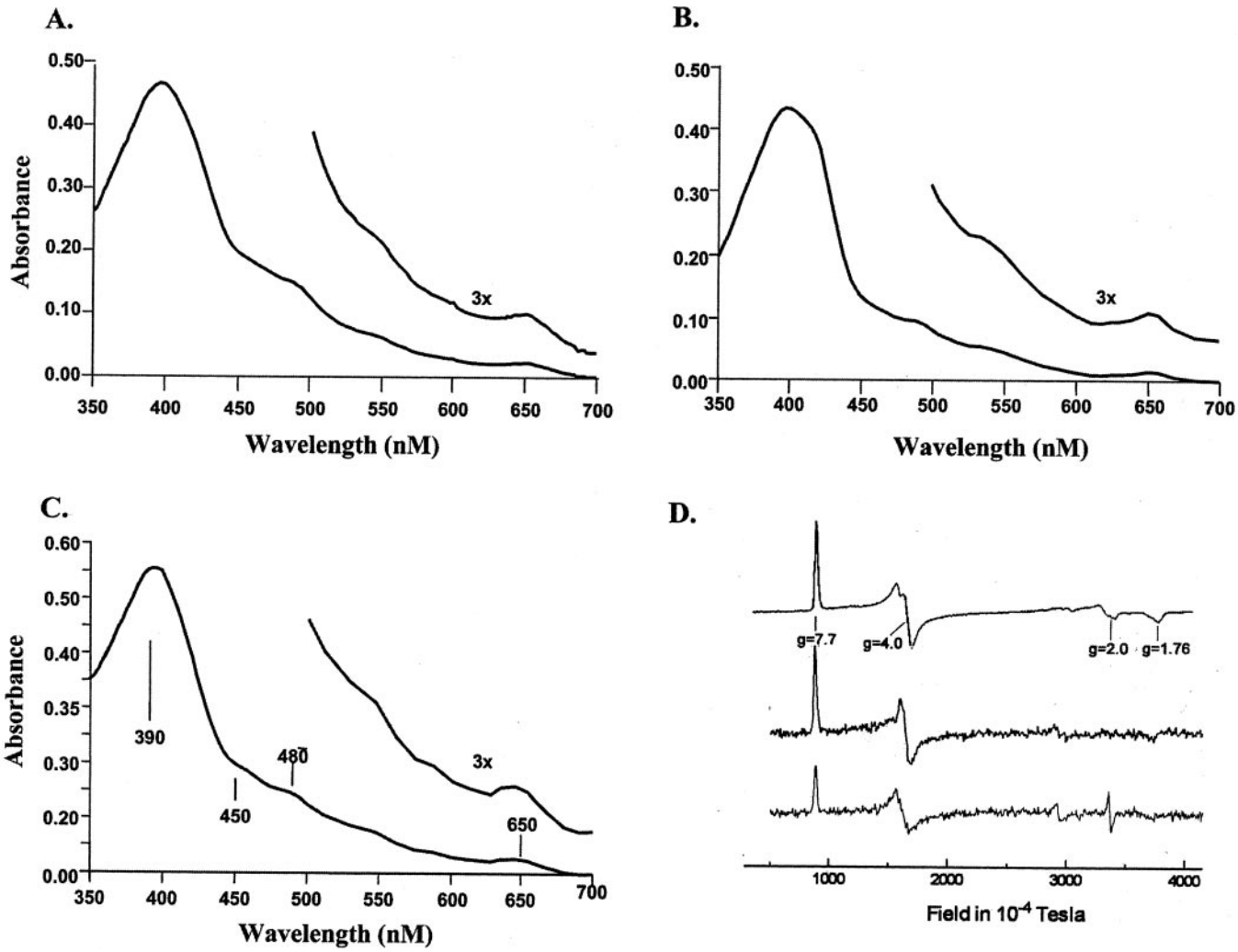

FIGURE 3. Light absorbance spectral analysis of NOS oxyFMN proteins from murine iNOS (*A*), human eNOS (*B*), and rat nNOS (*C*). *A*, spectra of iNOS oxyFMN, recorded in 40 mM EPPS, pH 7.6, containing 5% glycerol (v/v) 5 mM 2-mercaptoethanol, pH 7.6, 10 μM H_4B, and 1 mM L-Arg at 28 °C had maximum absorbance at 390 nm, typical of high spin penta-coordinate heme protein. *B* and *C*, spectra of human eNOS and rat nNOS oxyFMN, recorded in 40 mM Bis-tris-propane, pH 7.6, containing 5%glycerol, 5 mM 2-mercaptoethanol, 10 μM H_4B, and 1 mM L-Arg showed the predominant high spin heme in human eNOS with some low spin heme present, whereas the heme in nNOS is completely high spin and centered at 390 nm. In addition, all these spectra showed typical flavin (FMN) peaks at 450 and 480 nm and a characteristic high spin ferriheme charge transfer band at 650 nm. *Panel D* (*top trace*) shows the electron paramagnetic resonance spectrum of nNOS oxyFMN construct at a concentration of 45 μM recorded at 10 K. Instrument settings were: microwave power, 2 milliwatts; modulation amplitude, 10 gauss; modulation frequency, 100 kHz; microwave frequency, 9.47 GHz; magnetic field scan, 0.4 millitorr; field center, 0.23 millitorr. The spectrum is dominated by a single high spin species with features at g = 7.7, 4.0 and 1.76. Axial high spin heme at g = 6 and low spin heme at g = 2.4 are almost undetectable, and there is very little free radical at g = 2. The conditions for the lower two traces are the same except that the temperature is 15 K, and the gain has been increased. The *middle trace* shows a spectrum of oxidized iNOS oxyFMN construct; the sample concentration was ~15 μM. The *lower trace* shows a second spectrum of nNOS oxyFMN complex after reduction with dithionite and partial reoxidation by exposure to air; the heme is only about 50% in the ferric state. An FMN radical is visible at g = 2.

purification index. The iNOS construct migrates as a single majority band at 69 kDa on SDS-PAGE, with a minority band at 50 kDa due to a cleavage product and a 15.7-kDa band from co-expressed CaM. The eNOS and nNOS oxyFMN preparations have additional minor bands at 50–55 kDa (Fig. 4, *inset*). The estimated molecular mass for nNOS oxyFMN is ~75 kDa.

Fig. 5*a* shows a comparison between spectra of oxidized iNOS holoenzyme, oxygenase domains, and oxyFMN constructs in the presence of H_4B and arginine. All three constructs are primarily high spin with a Soret maximum of ~395 nm and a well developed 650-nm band. The oxygenase domain spectrum lacks flavin features at 450 and 480 nm, whereas the holoenzyme spectrum has approximately twice the contribution from flavin relative to heme of the oxyFMN spectrum.

Fig. 5*b* shows the effect of arginine addition on the spectrum of iNOS oxyFMN construct. Enzyme isolated in the presence of arginine diluted with arginine-free buffer is in a mixed spin state as indicated by the Soret shoulder at 420 nm; omission of arginine during purification produces a low quality preparation. Treatment with imidazole produces a characteristic low spin spectrum with a sharp Soret band at 425 nm. Dialysis with a change of buffers removes both imidazole and any remaining traces of arginine, which is displaced by imidazole binding, producing a mixed spin preparation with a Soret band at maximum near 400 nm and a pronounced shoulder at 420 nm. The addition of excess arginine produces a completely high spin preparation with a broad Soret maximum below 400 nm lacking the 420-nm shoulder. The *inset* shows the difference spectrum of arginine binding to a dialyzed preparation in the presence of H_4B.

As judged by the effect of arginine on the heme Soret band, all three constructs bind H_4B and arginine. Arginine- and H_4B-replete iNOS and nNOS preparations are essentially 100% high spin by optical criteria, consistent with a high level of intactness of the cofactor and substrate binding sites and with accessibility of all sites to arginine and H_4B; a low spin minority species persists in eNOS preparations. The dissociation constant of L-arginine (K_d) for all three NOS oxyFMN constructs, as

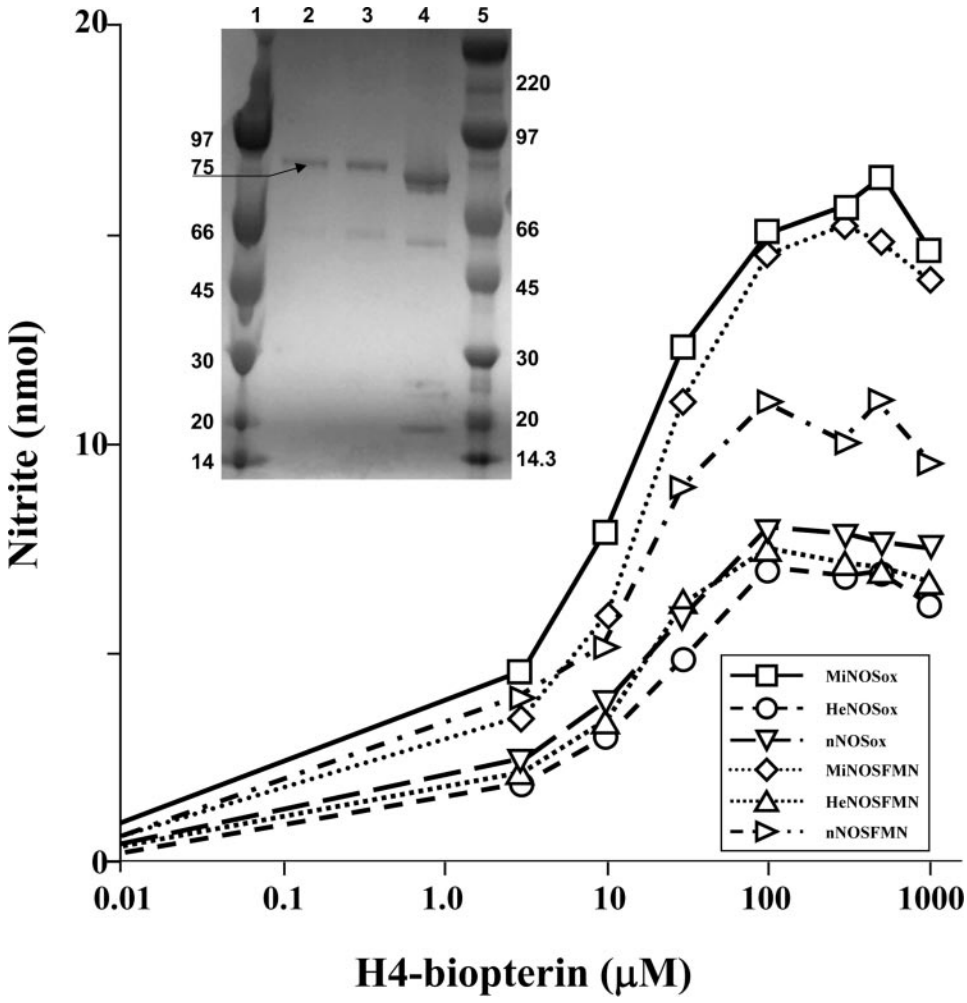

FIGURE 4. **Characterization of oxyFMN domains of human eNOS, rat nNOS, and murine iNOS by activity assay and SDS gel analysis.** Using an *E. coli* expression system, the oxyFMN constructs of wild-type human eNOS (residues 66–715), rat NOS (residues 291–947), and murine iNOS (residues 65–683) plus an N-terminal His_6 tag were generated and purified. OxyFMN activity was assessed by measuring H_2O_2-supported oxidation of NOHA. Protein samples were incubated for 30 min with the indicated concentrations of H_4B before initiating the reaction with H_2O_2. Nitrite values are the amount formed in 10 min at 37 °C. Data are representative of three experiments, each performed in triplicate. Oxygenase domain proteins from all three isoforms were included in the activity assay for comparison. The *inset* shows the SDS/PAGE analysis of the recombinant protein and confirms the size and the purity of the recombinant proteins. *Lanes 1* and *5*, low molecular weight LMW and rainbow markers from Amersham Biosciences Bioscience; *lane 2*, human eNOS oxyFMN; *lane 3*, rat nNOS oxyFMN; *lane 4*, murine iNOS oxyFMN.

determined by spectral perturbation analysis in presence of imidazole (progressive titration spectra is not shown, but titration spectra reflect low to high spin transitions as in the difference spectrum shown in the *inset* of Fig. 5*b*), indicates a high affinity site (K_d = 0.5–1.0 μM), confirming proper folding and dimerization of the oxygenase domain in these constructs.

Fig. 6 shows spectra of the iNOS oxyFMN construct recorded during stoichiometric titration with small aliquots of sodium dithionite solution. After stepwise addition of enough reductant to bleach the FMN bands at 455 and 480 nm, UV-visible spectra were recorded, and additional dithionite was added until FMN and heme were fully reduced, as judged by the spectra. The first electron into the construct reduces FMN to the blue neutral semiquinone state with loss of the oxidized FMN bands at 455 and 480 nm; at the same time, the weaker semiquinone bands can be observed near 560 and 600 nm. An additional band at 480 nm is difficult to resolve because it is overlapped by the stronger oxidized FMN band at 480 nm, but the broader semiquinone absorbance contributes additionally near 520 nm.

Further addition of reductant causes parallel bleaching of the semiquinone bands and conversion of the heme to the ferrous state. Heme reduction is visible as a red shift in the Soret and as loss of the high spin ferric charge transfer band at 650 nm; the latter is overlapped by the semiquinone bands. No red anionic semiquinone was detected. An additional cycle of oxidation and reduction produced spectra nearly identical to the original oxidized and reduced spectra, indicating that the construct was stable during the experiment. This method can be used to generate flavin semiquinone, whereas the heme is completely oxidized, but heme reduction and reduction of FMN to $FMNH_2$ cannot be separated in the iNOS construct, which has calmodulin tightly bound. This is probably due to equilibration of heme and FMN faster than the time scale of the experiment (about 1 min). The stability of the construct to cycles of oxidation/reduction is critical to the design of kinetics experiments to demonstrate rapid heme/FMN electron transfer.

Fig. 7 shows selected UV-visible spectra of iNOS FMN domain during a potentiometric titration. The midpoint potential for heme reduction is about −180 mV, slightly higher than observed in titrations of the holoenzyme or the independently expressed oxygenase domain. This can be readily observed in the Soret region; the peak position shifts from 390 nm to about 407 nm, and the band sharpens as the heme is reduced to the ferrous state. The charge transfer band at 650 nm disappears as the heme is reduced, and the ferrous α band region increases in intensity. Very similar results were obtained for the eNOS and nNOS constructs.

The oxidized FMN bands at 450 and 480 nm decrease in intensity as FMN is reduced to the semiquinone state. The blue neutral semiquinone is again most easily observed as a group of broad bands centered near 560, 590 and 620 nm and, in addition, by increased absorbance at 520 nm. The *inset* shows an expanded view of the titration of the 600–650-nm region, showing initially increasing intensity at 620 nm followed by loss in intensity at 620 and 650 as the potential is lowered further. The initial reduction of FMN occurs at approximately +70 mV; semiquinone reduction is essentially complete by −260 mV.

Fig. 8*a* shows a plot of the absorbance at 620 and 650 nm as a function

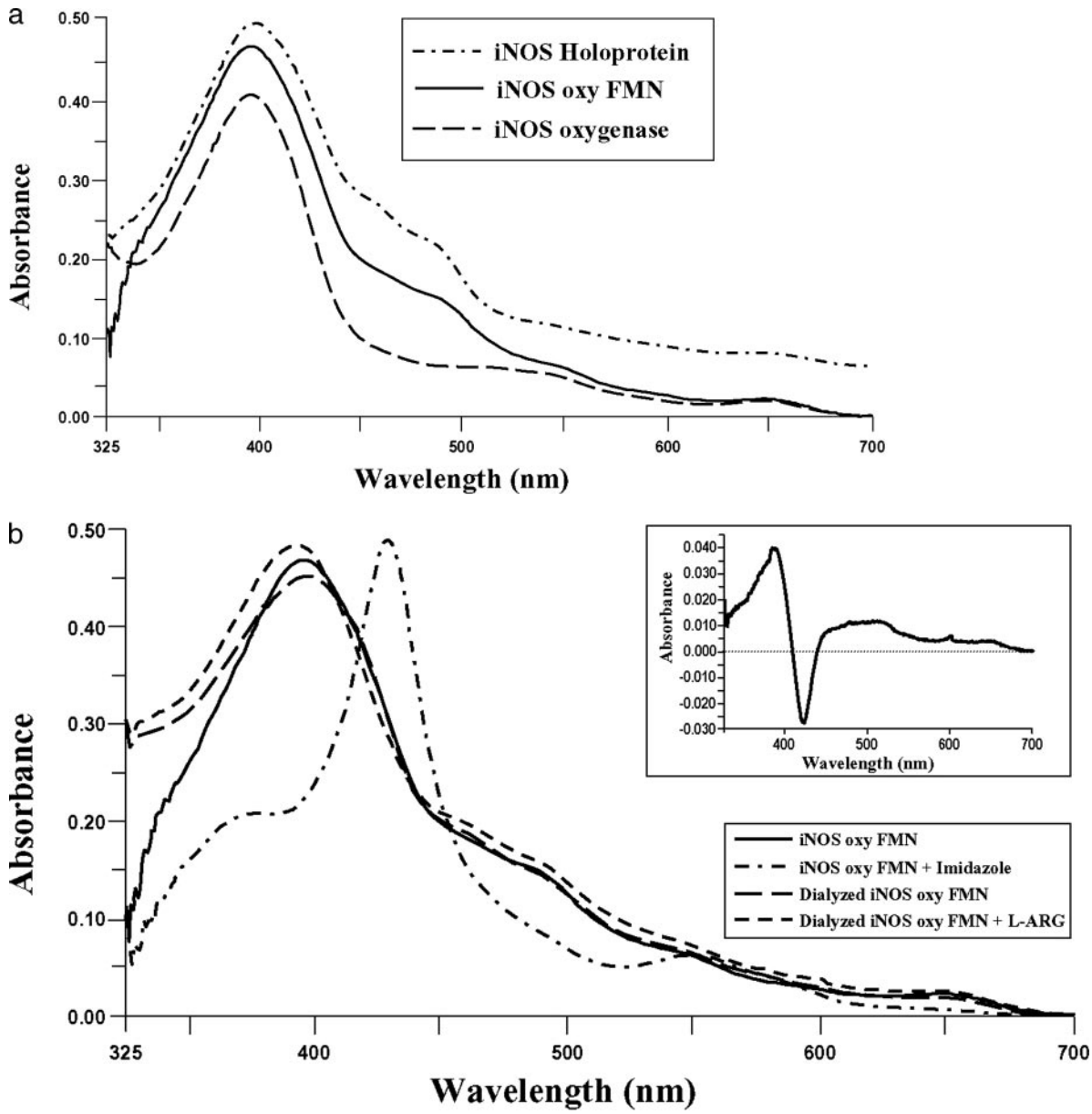

FIGURE 5. *a*, UV-visible spectra of iNOS oxyFMN construct compared with the corresponding oxygenase construct (flavin-free) and holoenzyme (replete with FAD and FMN). The spectrum of holoprotein has been displaced upwards to facilitate comparison of the relative contribution of flavin and heme bands. *b*, UV-visible spectra of iNOS oxyFMN construct showing ligand-induced spin state changes. As indicated in legend, spectra shown are of iNOS oxyFMN exposed to arginine during purification but after chromatography and dilution (admixed spin with 420 nm shoulder), after treatment with imidazole to replace arginine with a relatively weak binding ligand (sharp low spin peak at 425 nm), after removal of imidazole and trace arginine by dialysis with two changes of buffer (admixed spin with shoulder at 420 nm), and after the addition of saturating (1 mM) arginine (broad high spin peak at 390 nm).

of potential for spectra collected during the iNOS oxyFMN titration. The simulations are composed of two components, a ferriheme $n = 1$ component and an FMN semiquinone titrating as a thermodynamic transient. The potentials used to fit the 3 one-electron couples are −180 mV for the one-electron heme couple (E_{heme}), 70 mV for the FMN/FMNH$^{\bullet}$ couple (E_{1FMN}), and −180 mV for the FMNH$^{\bullet}$/$FMNH_2$ couple (E_{2FMN}).

Similar simulations of data collected at 455 and 520 nm are shown in Fig. 8*b*. The major contributions to the changes in absorbance at 455 nm are the heme Fe^{+2}/Fe^{+3} couple and the FMN/ FMNH$^{\bullet}$ couple. The data can be fit well with the potentials used to fit the data of Fig. 8*a*, but a slightly better fit was obtained with an E_{1FMN} of +50 mV. This difference is not significant. Because FMNH$^{\bullet}$ does not contribute significantly here, the FMNH$^{\bullet}$/$FMNH_2$ couple cannot be accurately determined at this wavelength, but it must be significantly lower than the FMN/FMNH$^{\bullet}$ couple.

The major contributions to the absorbance changes at 520 nm are the transient formation of semiquinone and the slightly greater contribution of ferric heme. The data have been fit with the same potentials as in Fig. 8*a*, except that the FMN/FMNH$^{\bullet}$ couple is again better fit at +50 mV. Similar results were obtained in titrations of nNOS (not shown).

Spectra taken during titration of eNOS and nNOS constructs are included in supplementary information. For eNOS and nNOS, calmodulin effects were examined by adding calmodulin and taking spectra at a few selected potentials. The results for both isoforms were consistent with a shift of about 20 mV to higher potential for both the heme and FMNH$^{\bullet}$/$FMNH_2$ couples, an effect at the edge of resolution in our experiments. An effect large enough to be responsible for the activation

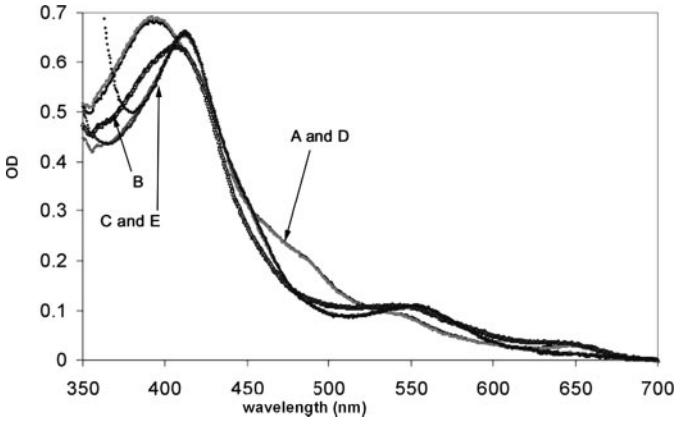

FIGURE 6. **UV-visible spectra taken during stepwise reductive titration of 8 μM iNOS oxyFMN construct replete with H_4B and arginine at pH 7.5 in 50 mM MOPS, 100 mM NaCl, 10% glycerol.** Reduced species were generated by adding continuous small aliquots of concentrated sodium dithionite solution (in 100 mM Tris base) until changes in absorbance at 480 nm were visible; spectra were then collected, and further additions were made. *A*, oxidized construct with no additions. The heme spectrum is indicative of almost completely high spin population (Soret and 650-nm charge transfer bands), and FMN is fully oxidized (strong 450- and 480-nm bands and no semiquinone features), consistent with epr results. *B*, oxyFMN iNOS partially reduced with a small aliquot of dithionite solution. Most of the change in the Soret region is due to the loss of the flavin band at ~384 nm; note that most of the heme charge transfer band at 650 is still present. FMN has been reduced to the semiquinone state, and the blue neutral species is visible at 600 and 520. Note that there is significant absorbance at 550–560 from blue neutral semiquinone. *C*, fully reduced with additional dithionite; note the loss of flavin bands and reduced Soret position. *D*, reoxidized with potassium ferricyanide; spectrum is nearly identical to *A*. *E*, re-reduced with excess dithionite; spectrum is almost identical to *C*.

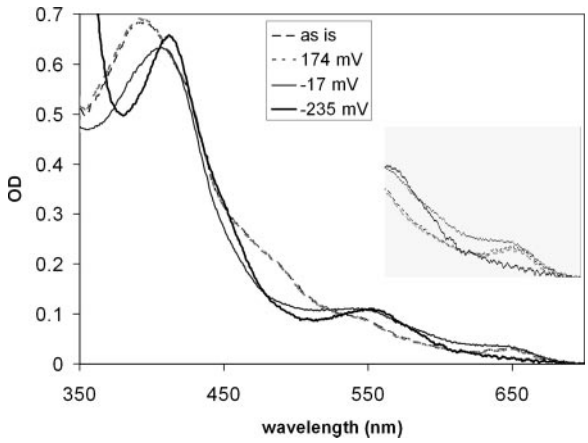

FIGURE 7. **Spectra taken during titration of iNOS oxyFMN construct showing oxidized FMN bands at 450 and 480 nm, red shift of heme Soret during reduction, and charge transfer and blue neutral semiquinone bands near 650 nm.** The *inset* shows details of charge transfer and blue neutral semiquinone band changes in the 600-650-nm region.

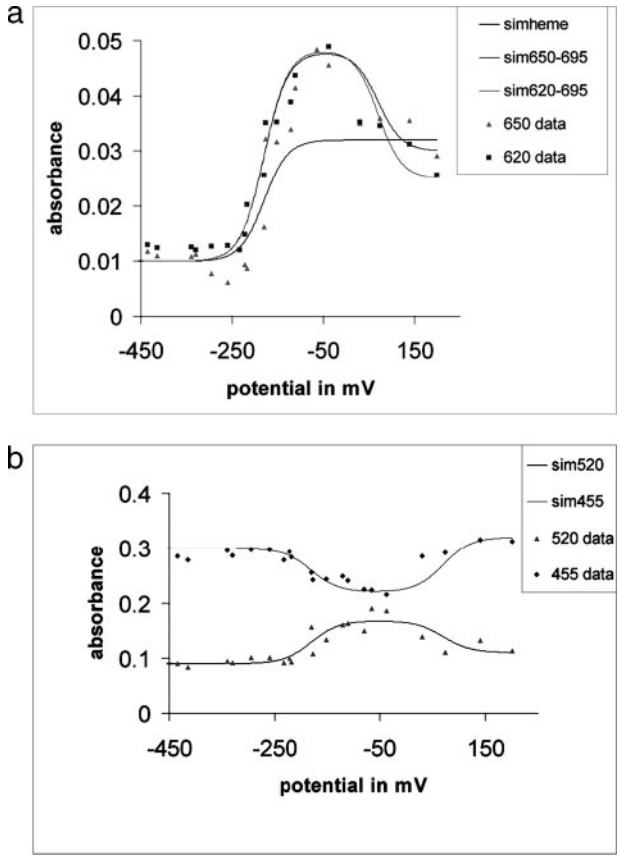

FIGURE 8. *a*, simulation of potentiometric titration of 620 and 650-nm absorbance of iNOS oxyFMN construct. Parameters for 620-nm simulation were: $Em_{1FMN} = +70$ mV, $Em_{2FMN} = -180$mV, Emheme $= -180$mV; semiquinone absorbance maximum $(C^*\epsilon) = 0.02344$, ferriheme absorbance maximum $= 0.015$. For the 650-nm simulation, the maximum contribution of the semiquinone was 0.018 and of ferriheme, 0.02 units, relative to the absorbance of the reduced enzyme. *simheme* represents the contribution of the heme to the absorbance at 650 nm. *b*, simulation of titration of 455- and 520-nm absorbance with potential. Parameters for 520-nm simulation were: $Em_{1FMN} = +70$ mV, $Em_{2FMN} = -180$ mV, Emheme $= 180$ mV. For the 455-mV simulation, the total contribution of ferriheme and semiquinone relative to reduced enzyme was -0.09 units, and the contribution of oxidized FMN was 0.1 units.

TABLE 1

Midpoint potentials at pH 7.5 of electron carriers in oxyFMN constructs

Potentials are accurate to within 20 mV for eNOS and nNOS and 10 mV for iNOS; heme potential is from fits to a single component. sq/hq, semiquinone/hydroquinone couple; ox/sq, oxidized/semiquinone couple.

	FMN ox/sq	FMN sq/hq	Heme
eNOS	0 mV	−210 mV	−210 mV
iNOS	+70 mV	−180 mV	−180 mV
nNOS	+50 mV	−180 mV	−190 mV

of electron transfer is ruled out, consistent with previous results with holoenzyme (15).

The results for titrations of iNOS, eNOS, and nNOS are summarized in Table 1. The potentials are generally similar, although the details are slightly different. In general, the first one-electron reduction of the FMN occurs at high potential as in holoenzyme and in reductase constructs. The second single electron reduction of FMN and heme reduction are nearly isopotential. The eNOS construct contains a significant minority species that is low spin in the presence of arginine.

Fig. 9 shows effects of interdomain interactions on EPR signals of the high spin ferriheme. The *three top traces* are the g_{max} features of nNOS constructs; the asymmetry is due to the details of strain broadening. The central peak is the g_{max} signal from a nNOS oxygenase preparation replete with arginine and H_4B; $g_{max} \sim 7.72$. The *left peak* is the corresponding signal from a nNOS oxyFMN preparation. g_{max} for this peak is ~7.72. Although the peak position of the strain broadened line is only slightly shifted to high field relative to the oxygenase construct, the line is significantly sharpened, and the low field edge is noticeably shifted to the left (see "Discussion"). The *right hand peak* is the g_{max} signal from the same nNOS oxyFMN preparation in the presence of Ca^{+2}/CaM. The peak has shifted downfield to $g \sim 7.69$, and the low field side of the line is broader. We attribute this shift in peak position and line shape to the effect of calmodulin-induced association of the FMN binding domain on the ligand geometry of the heme. This is the first report of a calmodulin effect on the spectrum of heme in any NOS construct.

The two lower spectra show the g_{max} features of iNOS oxyFMN

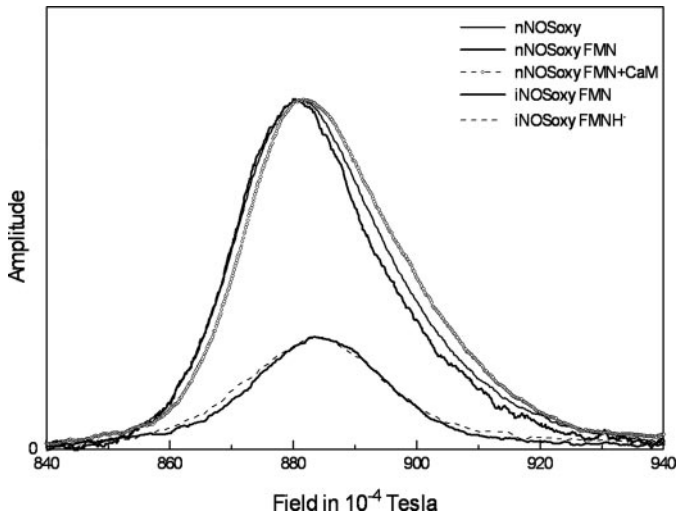

FIGURE 9. **EPR spectra in the g_{max} region of high spin ferriheme showing the effects of interactions between the FMN and heme binding domains of oxyFMN constructs.** Instrument settings were: microwave power, 2 milliwatts; modulation amplitude, 10 gauss; modulation frequency, 100 kHz; microwave frequency, 9.51 GHz; magnetic field scan, 0.02 millitorr; field center, 0.086 millitorr; spectra were recorded at 15 K. *Top traces* show the effect of CaM binding on the heme EPR signals of nNOS constructs. *Left trace*, nNOS oxyFMN construct. *Center trace*, nNOS oxygenase construct. *Right hand trace*, nNOS oxyFMN construct after the addition of calcium and calmodulin. Concentrations of all samples were ~45 μM. *Lower traces* show the effect of FMN radical formation on the EPR spectrum of iNOS oxyFMN ferriheme. *Solid trace*, oxidized iNOS oxyFMN construct. *Dashed trace*, iNOS oxyFMN construct after one cycle of reduction with dithionite and air reoxidation. Concentration of iNOS oxyFMN construct was ~15 μM. Small adjustments of the gains of two traces were made to facilitate comparison of line shapes and traces; the amplitude of the *upper left trace* (nNOS oxyFMN) was decreased by 10%, and the amplitude of the *lower dashed trace* (iNOS oxyFMN plus calmodulin) was increased by 10%.

construct. Because the iNOS construct must be coexpressed with a calmodulin, we couldn't perform the analogous experiment to demonstrate the change in the heme environment triggered by CaM binding. The *solid trace* at $g_{max} \sim 7.72$ is very close in peak position to the nNOS oxyFMN construct position after the addition of CaM. The *dashed line* shows the g_{max} feature of the same preparation after the addition of 2 μl of saturated dithionite solution to the 250-μl sample. This generated a FMNH• radical in about ⅓ of the enzyme molecules. The high field side of the g_{max} line is broadened in this sample. To produce an effect of this magnitude in a sample with only partial conversion to the radical state, a magnetic interaction of 5–10 gauss would be required. The spectrum of the flavin radical at $g = 2$ is also broadened; we hope to present an analysis of the magnetic interactions in a subsequent communication.

DISCUSSION

The results presented here demonstrate that two-domain oxyFMN constructs of all three mammalian NOS isoforms can be expressed in *E. coli* and are well folded and bind functional prosthetic groups. The oxyFMN construct is designed to be the "output state" counterpart of the three-domain reductase construct and as such should be of value in probing the mechanism of the enzyme. The purpose of this study was to establish that such constructs could be expressed and purified in qualities and quantities suitable for detailed structural and functional studies. In addition, characterization of the constructs was undertaken to determine some critical parameters for internal electron transfer reactions.

It is clear from the spectroscopic and enzymology results that the oxygenase domain is stable and functional. By spectroscopic criteria, preparations of all three constructs are superior to most holoenzyme preparations in that they are homogeneous, bind substrate and cofactors stoichiometrically, and do not contain significant amounts of denatured material.

The titration results are of special interest. The FMN semiquinones are stable and are the blue neutral forms as in the holoenzymes. The midpoint potentials of the heme and the $FMNH^{\bullet}/FMNH_2$ couple appear, however, to be slightly above −200 mV in all three cases. This is 60 mV or more greater than the potentials obtained using individual domains and holoenzyme preparations, a modest but significant difference corresponding to a 1 order of magnitude change in equilibrium constants for electron transfer reactions. For example, in holoenzymes, typical values for arginine-replete heme and FMN are −240 mV for FeII/FeIII, 0 mV for $FMN/FMNH^{\bullet}$, and −250 mV for $FMNH^{\bullet}/FMNH_2$ (15). The FMN couples were reported by Noble *et al.* (17) to be about −50 and −275 mV in isolated reductase constructs.

In summary, as in holoenzyme the $FMNH^{\bullet}/FMNH_2$ and heme couples are an approximately isopotential group, whereas the $FMN/FMNH^{\bullet}$ couple is too high in potential to be an effective heme reductant in steady state experiments. This need not rule out the possibility of generating a transient one-electron reduced FMN species that would effectively reduce the heme by rapid electrochemical or photochemical methods.

Observation of higher potentials in a construct in which the electron carriers may be more exposed to solvent should not be surprising. The heme in these constructs, however, has a potential higher than that reported for individually expressed oxygenase domains (−220 mV in the presence of arginine) (38). This appears to be a special property of the construct and may reflect interactions between the domains. In nNOS and iNOS constructs, arginine generates nearly complete high spin ferriheme; small amounts of low spin sometimes persist. As Fig. 3 indicates, the eNOS construct is less homogeneous spectrally and contains a significant low spin component corresponding to about 30% of the total heme in the presence of arginine.

Some differences in opinion exist concerning the effects of arginine. Presta *et al.* (38) report little or no effects of arginine on apparent midpoint potentials of iNOS oxygenase domain constructs. We found that arginine shifted the midpoint potential of heme in iNOS and nNOS holoenzyme by at least 60 mV; preparations free of H_4B did not titrate as a single component, suggesting a range of conformations and/or dimerization states with different properties (15, 41).

It is particularly interesting to note that the potentials of both the heme and the $FMNH^{\bullet}/FMNH_2$ couple in the iNOS and nNOS constructs, which are the most homogeneous and native of the three expressed so far and are both slightly higher than the potentials of these carriers in holoenzymes but remain approximately isopotential. This suggests the possibility that the ~60-mV shift we observe reflects the effects of FMN/oxygenase domain interactions and that these interactions developed to retain the reversibility of the FMN/heme electron transfer in the absence of a reaction (*e.g.* NO production) pulling the equilibrium toward the oxygenase site. Potential differences are not strong evidence of FMN-heme interaction, but interactions between the two domains are a possible explanation for small differences in the observed potentials.

In contrast, the spectral evidence for interactions between the domains is very strong. The calmodulin-driven shifts in the EPR peak position and line shape of the nNOS oxyFMN complex shown in Fig. 9 indicate changes in the ratio of the rhombic and axial zero field splitting parameters E and D. As E/D increases, $\mathbf{g}x$ and $\mathbf{g}y$ split about 6; $\mathbf{g}z$ and $(\mathbf{g}x + \mathbf{g}y)/2$ decrease as a second-order effect. High spin ferrihemes are well described by the $S = 5/2$ spin Hamiltonian $D\{Sz^2 - \frac{1}{3}[S(S+1)]\} + E(Sx^2 - Sy^2)$, where E and D reflect differential admix-

ture of low-lying states into the ground state $^6A_1$ sextet by spin-orbit coupling because of tetragonal and rhombic splitting of the t_{2g} d orbitals (see for example Ref. 37).

The strain-broadened line shape is produced by distributions of E/D centered around 0.083 that inherently produce a sharper high field side to the line because the dependence of the field position on E/D becomes weaker as E/D increases. All NOS EPR spectra observed so far result from E/D ratios in the range 0.058–0.088. In this case E/D is probably close to the upper limit which can be obtained with thiolate ligation and the underlying molecular geometry.

It is not surprising that CaM-driven association of the FMN and oxygenase domains affects the distribution of E/D at the heme iron. Interaction of the surface charge distributions adjacent to the prosthetic groups is the likely source of the observed small distortion of the heme environment. CaM does not produce a comparable effect in holoenzyme, probably because the fraction of molecules in which the FMN domain associates with the heme site is too small.

The broadening of the ferriheme g_{max} line produced by formation of FMN radical in iNOS oxyFMN is less obvious than the broadening of the radical because the heme line width at g_{max} is about twice that of the radical line width and because only about ⅓ of the heme interacts with radical, whereas all or nearly all of the radical interacts with heme. Interactions of 5–10 gauss are likely to be due primarily to dipole-dipole coupling (*e.g.* Ref. 42). The interactions acquire anisotropy from both the heme g tensor and the $(1–3\cos^2\Theta)$ dependence of dipolar coupling, where Θ is the angle between the magnetic field and the interspin vector; such interactions have an r^{-3} distance dependence. We hope eventually to obtain detailed distance and orientation information from simulation of spectra, but it is clear that the heme-FMN distance is in the 10–15-Å range, favorable for electron transfer. This close association would be impossible for a holoenzyme conformation analogous to the reported crystal structure of nNOS reductase complex.

In isolated domains the potentials of the flavin couples have been reported to be somewhat lower than our results in holoenzymes. Reductase domain and holoenzyme FMN/FMNH$^\bullet$ couples are high potential and similar to these couples in oxyFMN constructs (17), but in isolated FMN domains the FMN/FMNH$^\bullet$ couples are significantly lower (−180 to −190 mV) in potential (18). The FMNH$^\bullet$/FMNH$_2$ couples are also lower in isolated FMN binding domains (−300 to −320 mV), but this effect is much more modest. This couple in holoenzymes is about midway between the values obtained in isolated domains and those obtained here in oxyFMN complexes. These effects may be coincidental, but the moderate shifts in potential are those expected if some redox energy is exchanged to drive the association and dissociation of domains. For example, if reduced FMN destabilized the input state, the FMNH$^\bullet$/FMNH$_2$ couple would be lower in potential in the reductase complex. If reduced FMN promotes formation of the output state and oxidized FMN promotes its dissociation, the FMNH$^\bullet$/FMNH$_2$ couple would be higher in potential in the oxyFMN complex.

An analogous FMN domain/oxygenase construct has been studied in P450-BM3, but the properties of that system are very different (43). Most obviously, the oxygenase domains of P450 and NOS are not even distantly homologous, and BM3 lacks a calmodulin binding site. The interdomain linker in the BM3 construct is sensitive to proteolysis and has been degraded in the crystal structures presented (43). In addition, the mechanism of the BM3 system is very different than that of NOS or P450 reductase in that the FMN binding domain of the BM3 system has a low potential FMNH$^\bullet$/FMN couple, and the semiquinone is the physiological reductant. The FMN binding domain in the BMN3 system is a flavodoxin homolog, but it has a very different interdomain interaction surface (43), lacking the flavodoxin-derived conserved clusters of negative charge found in P450 reductase (22) and NOS (24, 44). It will be of interest to compare the structures and mechanisms of the output states of the NOS and BM3 systems.

In conclusion, the oxyFMN constructs of all three mammalian NOS isoforms have been expressed as stable proteins with activity and interesting properties. We have observed the first direct effects of CaM on NOS heme spectra and the first indications of FMN-heme magnetic coupling. They appear to be good candidates for further kinetic and structural studies of the NOS output state.

Acknowledgments—We gratefully acknowledge the assistance of Prof. Charles Scholes and Prof. Tomoko Ohnishi with epr experiments. We thank Lesa Hall, Veterans Affairs Medical Center, Durham, NC, for graphics.

REFERENCES

1. Hibbs, J. B., Taintor, R. R., and Vavrin, Z. (1987) *Science* **235,** 473–476
2. Marletta, M. A. (1993) *J. Biol. Chem.* **268,** 12231–12234
3. Stuehr, D. J. (1991) *J. Biol. Chem.* **266,** 6259–6263
4. Nathan, C., and Xie, Q. W. (1994) *Cell* **78,** 915–918
5. Roman, L. J., Martásek, P., and Masters, B. S. S. (2002) *Chem. Rev.* **102,** 1179–1190
6. Sessa, W. C. (2005) *Mem. Inst. Oswaldo Cruz* **100,** Suppl. 1, 15–18
7. Ghosh, D. K., Abu-Soud, H. M., and Stuehr, D. J. (1996) *Biochemistry* **35,** 1444–1449
8. Crane, B. R., Arvai, A. S., Ghosh, D. K., Wu, C., Getzoff, E. D., Stuehr, D. J., and Tainer, J. A. (1998) *Science* **279,** 2121–2126
9. McMillan, K., Bredt, D. S., Hirsch, D. J., Snyder, S. H., Clark, J. E., and Masters, B. S. (1992) *Proc. Natl. Acad. Sci. U. S. A.* **89,** 11141–11145
10. Kwon, N. S., Nathan, C. F., and Stuehr, D. J. (1989) *J. Biol. Chem.* **264,** 20496–20501
11. Bredt, D. S., Hwang, P. M., Glatt, C. E., Lowenstein, C., Reed, R. R., and Snyder, S. H. (1991) *Nature* **351,** 714–718
12. Bredt, D. S., and Snyder, S. H. (1990) *Proc. Natl. Acad. Sci. U. S. A.* **87,** 682–685
13. Siddhanta, U., Presta, A., Fan, B., Wolan, D., Rousseau, D. L., and Stuehr, D. J. (1998) *J. Biol. Chem.* **273,** 18950–18958
14. Abu-Soud, H. M., Yoho, L. L., and Stuehr, D. J. (1994) *J. Biol. Chem.* **269,** 32047–32050
15. Gao, Y. T., Smith, S. M. E., Ghosh, D., Guillemette, J. G., and Salerno, J. C. (2004) *J. Biol. Chem.* **279,** 18759–18766
16. Daff, S., Noble, M. A., Craig, D. H., Rivers, S. L., Chapman, S. K., Munro, A. W., Fujiwara, S., Rozhkova, E., Sagami, I., and Shimizu, T. (2001) *Biochem. Soc. Trans.* **29,** 147–152
17. Noble, M. A., Munro, A. W., Rivers, S. L., Robledo, L., Daff, S. N., Yellowlees, L. J., Shimizu, T., Sagami, I., Guillemette, J. G., and Chapman, S. K. (1999) *Biochemistry* **38,** 16413–16418
18. Garnaud, P. E., Koetsier, M., Ost, T. W. B., and Daff, S. N. (2004) *Biochemistry* **43,** 11035–11044
19. Salerno, J. C., Harris, D. E., Irizarry, K., Patel, B., Morales, A. J., Smith, S. M., Martasek, P., Roman, L. J., Masters, B. S., Jones, C. L., Weissman, B. A., Lane, P., Liu, Q., and Gross, S. S. (1997) *J. Biol. Chem.* **272,** 29769–29777
20. Jones, R. J., Smith, S. M. E., Gao, Y. T., DeMay, B. S., Mann, K. J., Salerno, K. M., and Salerno, J. C. (2004) *J. Biol. Chem.* **279,** 36876–36883
21. Roman, L. J., Martasek, P., Miller, R. T., Harris, D. E., de La Garza, M. A., Shea, T. M., Kim, J. J., and Masters, B. S. (2000) *J. Biol. Chem.* **275,** 29225–29232
22. Wang, M., Roberts, D. L., Paschke, R., Shea, T. M., Masters, B. S. S., and Kim, J. J. (1997) *Proc. Natl. Acad. Sci.* U. S. A. **94,** 8411–8416
23. Zhang, J., Martasek, P., Paschke, R., Shea, T., Masters, B. S. S., and Kim, J.-J. P. (2001) *J. Biol. Chem.* **276,** 37506–37513
24. Garcin, E. D., Bruns, C. M., Lloyd, S. J., Hosfield, D. J., Tiso, M., Gachhui, R., Stuehr, D. J., Tainer, J. A., and Getzoff, E. D. (2004) *J. Biol. Chem.* **279,** 37918–37927
25. Ghosh, D. K., and Salerno, J. C. (2003) *Front Biosci.* **8,** 193–209
26. Govindaraj, S., and Poulos, T. L. (1996) *J. Biol. Chem.* **272,** 7915–7921
27. Ghosh, D. K., Wu, C., Pitters, E., Moloney, M., Werner, E. R., Mayer, B., and Stuehr, D. J. (1997) *Biochemistry* **36,** 10609–10619
28. Fedorov, R., Vasan, R., Ghosh, D. K., and Schlichting, I. (2004) *Proc. Natl. Acad. Sci. U. S. A.* **101,** 5892–5897
29. Roman, L. J., Sheta, E. A., Martasek, P., Gross, S. S., Liu, Q., and Masters, B. S. S. (1995) *Proc. Natl. Acad. Sci. U. S. A.* **92,** 8428–8432
30. Ghosh, D. K., Rashid, M. B., Crane, B., Taskar, V., Mast, M., Misukonis, M. A., Weinberg, J. B., and Eissa, N. T. (2001) *Proc. Natl. Acad. Sci. U. S. A.* **98,** 10392–10397
31. Newman, E., Spratt, D. E., Mosher, J., Cheyne, B., Montgomery, H. J., Wilson, D. L.,

Weinberg, J. B., Smith, S. M. E., Salerno, J. C., Ghosh, D. K., and Guillemette, J. G. (2004) *J. Biol. Chem.* **279,** 33547–33557
32. Ghosh, D. K., Crane, B. R., Ghosh, S., Wolan, D., Gachhui, R., Crooks, C., Presta, A., Tainer, J. A., Getzoff, E. D., and Stuehr, D. J. (1999) *EMBO J.* **18,** 6260–6270
33. Pufahl, R. A., Wishnok, J. S., and Marletta, M. A. (1995) *Biochemistry* **34,** 1930–1941
34. Dutton, P. L. (1978) *Methods Enzymol.* **54,** 411–435
35. Stuehr, D. J., and Ikeda-Saito, M. (1992) *J. Biol. Chem.* **267,** 20547–20550
36. McMillan, K., and Masters, B. S. S. (1993) *Biochemistry* **32,** 9875–9880
37. Salerno, J. C., McMillan, K., and Masters, B. S. S. (1996) *Biochemistry* **35,** 11839–11845
38. Presta, A., Weber-Main, A. M., Stankovich, M. T., and Stuehr, D. J. (1998) *J. Am. Chem. Soc.* **120,** 9460–9465
39. Raman, C. S., Li, H., Martasek, P., Kral, V., Masters, B. S. S., and Poulos, T. L. (1998) *Cell* **95,** 939–950
40. Fischmann, T. O., Hruza, A., Niu, X. D., Fossetta, J. D., Lunn, C. A., Dolphin, E., Prongay, A. J., Reichert, P., Lundell, D. J., Narula, S. K., and Weber, P. C. (1999) *Nat. Struct. Biol.* **6,** 233–242
41. Smith, S. M. E., and Salerno, J. C. (2000) *Nitric Oxide* **4,** 224
42. Ruzicka, F. J., Beinert, H., Schepler, K. L., Dunham, W. R., and Sands, R. H. (1975) *Proc. Natl. Acad. Sci. U. S. A.* **72,** 2886–2890
43. Sevrioukova, I. F., Li, H., Zhang, H., Peterson, J. H., and Poulos, T. L. (1999) *Proc. Natl. Acad. Sci. U. S. A.* **96,** 1863–1868
44. Harris, D., Smith, S. M. E., Brown, C., and Salerno, J. C. (1997) in *Oxygen Homeostasis and Its Dynamics*, Vol. 1, Keio University Symposia for Life Sciences and Medicine (Ishimura, Y., Shimada, H., and Suematsu, M., eds) pp. 289–297, Springer-Verlag, Tokyo